JACS
JOURNAL OF THE AMERICAN CHEMICAL SOCIETY

Article

pubs.acs.org/JACS

Light-Triggered Eradication of *Acinetobacter baumannii* by Means of NO Delivery from a Porous Material with an Entrapped Metal Nitrosyl

Brandon J. Heilman, Jessica St. John, Scott R. J. Oliver, and Pradip K. Mascharak*

Department of Chemistry and Biochemistry, University of California - Santa Cruz, Santa Cruz, California 95064, United States

Supporting Information

ABSTRACT: A photoactive manganese nitrosyl, namely $[Mn(PaPy_3)(NO)](ClO_4)$ ({Mn-NO}), has been loaded into the columnar pores of an MCM-41 host. Strong interaction between the polar nitrosyl and the −OH groups on the host wall leads to excellent entrapment of the NO donor within the porous host. With the aluminosilicate-based host (Al-MCM-41), the loading is further enhanced due to electrostatic interaction of the cationic species with the aluminum sites. The extent of loading has been determined via analytical techniques including N_2 adsorption/desorption isometry. Powder X-ray diffraction studies on the loaded materials afford patterns typical of an ordered mesoporous silicate consisting of a hexagonal array of unidimensional channels (with slight loss of crystallinity). Elemental mapping of the loaded particles confirms the incorporation of {Mn-NO} into the porous MCM-41 structure and attests to the homogeneity of the guest molecule distribution throughout individual particles. When suspensions of the loaded materials in saline solution are exposed to low-power (10−100 mW) visible light, rapid release of NO is observed. With continuous exposure, a steady release of 50−80 μM of NO is attained with 5 mg of material/mL buffer within 5 min, and the NO flux is maintained for a period of ∼60 min. Rapid bursts of 5−10 μM NO are noted with short light pulses. Loss of either the nitrosyl or its photoproduct(s) from these materials in biological media is minimal over long periods of time. The NO release profiles suggest potential use of these powdery biocompatible materials as NO donors where the delivery of NO (a strong antibiotic) could be controlled via the exposure of light. Such prediction has been confirmed with the successful eradication of both drug-susceptible and drug-resistant *Acinetobacter baumannii* in a soft-tissue infection model through light-triggered NO delivery.

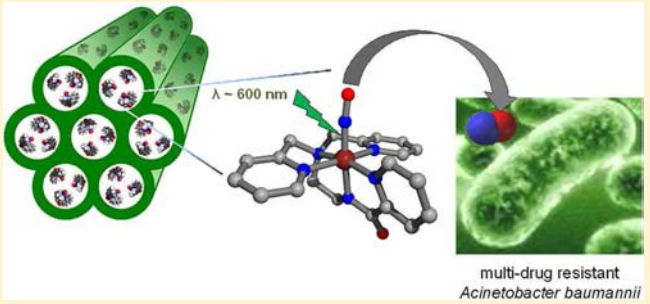

INTRODUCTION

Nitric oxide (NO) has been recognized through numerous studies as a potent antibiotic even against highly drug-resistant bacterium such as methicillin-resistant *Staphylococcus aureus* (MRSA).[1−3] NO exerts its toxic effect by directly nitrosating DNA and proteins or by combining with reactive oxygen species (such as superoxide and peroxide) and oxidizing the same targets as well as a range of lipids in the cellular membrane.[4] Because NO has a large number of targets and the bacteria can employ few mechanisms to thwart its actions, bacteria rarely exhibit resistance to NO.[5] The efficacy of gaseous NO in treating chronic infection has been demonstrated in an earlier study where delivery of gaseous NO to a nonhealing diabetic leg ulcer effectively eradicated the infection which had been resistant to various treatments over a two year period.[6] Since then, several groups have utilized NO to reduce bacterial loads in infected wounds.[7−9] Difficulties in the delivery of the toxic (and reactive) gaseous NO to selected targets have inspired the development of a diverse array of methodologies,[2,10] utilizing numerous variations on gaseous delivery systems,[6,11] creams,[12] polymeric materials[13−15] and inorganic solids.[2,13,16−20] Most of these delivery systems initiate NO release under thermal,[13,18] water-,[19,20] or pH-based[21] stimuli. Very few studies have utilized light as the trigger for NO release to infected sites.[22,23]

The rise of drug-resistant bacteria has sparked great interest in the design of novel approaches to combat the diverse and numerous mechanisms which bacteria employ to provide themselves protection against the action of antibacterial therapeutics.[24] New drug scaffolds continue to be developed, and as their complexity grows, the amount of resources spent on their development grows as well.[25] However, there remains a subset of bacterial pathogens which has developed resistance to nearly the entire spectrum of antibiotics available to researchers and are deemed multidrug-resistant (MDR) bacteria. Furthermore, phenotypic resistance such as the formation of bacterial biofilms can also impart decreased susceptibility to nearly all forms of known antibiotics.[26] The treatment of organisms displaying intrinsic and/or phenotypic antibiotic resistance is therefore extremely limited in the realm of traditional antibiotics. The application of NO could be more promising since (a) MDR bacteria seldom show resistance

Received: March 7, 2012
Published: May 11, 2012

   dx.doi.org/10.1021/ja3022736 | J. Am. Chem. Soc. 2012, 134, 11573−11582

toward NO and (b) NO is capable of dispersing biofilms quite effectively.[27]

There are several species of bacterial pathogens that seem to have a genetic disposition toward developing broad-spectrum antibiotic resistance. Just as the bacterium *S. aureus* has nearly become synonymous with resistance to β-lactam-based antibiotics (60% of hospital-acquired *S. aureus* isolates are methicillin-resistant),[28] the bacterium, *Acinetobacter baumannii*, has similarly become synonymous with multidrug resistance (14% of clinical isolates were resistant to eight different antibiotics in one study).[29−31] The high transmission rate of infection by *A. baumannii*, especially in hospital settings, compounds the problematic nature of infection by MDR *A. baumannii* strains.[32,33] Following the admission of coalition soldiers wounded during tours in Operation Iraqi Freedom and Operation Enduring Freedom in Afghanistan to military and civilian hospitals, there was a large increase in the occurrence of *A. baumannii* infection among admitted patients in these hospitals.[34−36] Our interest in utilizing NO-donating materials to tackle bacterial pathogens[2,22,37] thus prompted us to explore the possibility of studying the effects of NO on *A. baumannii* and evaluate the possibility of using a photosensitive NO-delivery platform in the treatment of *A. baumannii* infection.

Silicate-based porous materials such as zeolites and molecular sieves have recently been used as the delivery systems for NO to biological targets. This platform is an attractive option for NO administration since the silicate carrier is chemically inert and exhibits no toxicity in the body. One of the first systems, described by Wheatley and co-workers in 2006, involved the coordination of NO to Co- or Zn-exchanged sites within the zeolite framework.[38,39] This system was capable of incorporating 1 mmol of NO per gram of zeolite-A and releasing nearly 100% of the incorporated NO over ∼40 min when in contact with moisture-rich air. Unfortunately, the amount of NO released by the material upon administration to the patient is very difficult to control, and this problem limits one's ability to properly decide the treatment regimen and avoid cellular damage due to exposure to excess NO. In this report, we describe the development of a photoactive system that releases bactericidal amounts of NO under the control of mW levels of visible light. The system relies on NO release from a photoactive manganese nitrosyl $[Mn(PaPy_3)(NO)](ClO_4)$ (abbreviated as {Mn-NO} hereafter, structure shown in Figure 1)[40] entrapped within the extended pores of the mesoporous material MCM-41. Although the incorporation of the metal nitrosyl into the pores of MCM-41 is initiated by simple diffusion, once inside, the polar nitrosyl interacts strongly with the terminal silanol groups lining the walls of the pores and is retained within the pores once the solvent evaporates. To further enhance the interaction of the guest molecule with the host framework, we have employed an aluminosilicate-based material which has a negatively charged host structure due to the substitution of aluminum for silicon atoms. The $[Mn(PaPy_3)(NO)]^+$ cations thus are entrapped inside the pores through strong electrostatic interactions. The metal complex utilized in this work is especially suited for this kind of host−guest chemistry as the photoproduct obtained after NO photolysis from the central manganese becomes doubly charged ($[Mn(PaPy_3)(H_2O)]^{2+}$) and therefore is expected to bind even more tightly to the walls of the porous host (no side effects or leakage of photoproducts). The loading efficiency and leaching of the guest nitrosyl from both silicate- and aluminosilicate-based host−guest systems have been determined in this study. The NO-releasing capacities of both materials have also been measured. As described in the following sections, these composite materials (powders) exhibit excellent antibacterial effects on the highly drug-resistant pathogen *A. baumannii* through the action of photoreleased NO under the control of light.

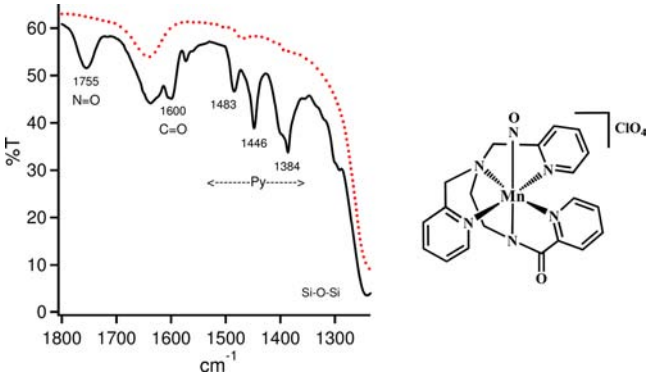

Figure 1. (Left panel): FTIR spectra of Si-MCM-41 (red dashed) and loaded (black solid) $\{Mn\text{-}NO\}_{200}$@Si-MCM-41 in KBr matrix. (Right panel): Structure of {Mn-NO}.

EXPERIMENTAL SECTION

Materials. MCM-41-type silicate and aluminosilicate molecular sieves were obtained from Sigma-Aldrich (St. Louis, MO). The Al-MCM-41 material was prewashed with 2 mM NaCl solution (by stirring the slurry for 30 min). It was then filtered and rinsed thoroughly with copious amounts of water. The sample was then dried in an 80 °C oven for 24 h. $[Mn(PaPy_3)(NO)](ClO_4)$ ({Mn-NO}) was synthesized by following published procedure.[40] Antibiotic susceptible *A. baumannii* freeze-dried culture (NCIMB 12457) and MDR *A. baumannii* (BAA-1605) were obtained from Microbiologics (St. Cloud, MN). BAA-1605 is a clinical isolate from the sputum of a soldier injured in Afghanistan and sent to a Canadian hospital in 2006. The strain showed resistance to 9 of 11 antibiotics tested.

Synthesis Safety Note. Transition metal perchlorates should be handled with great caution and be prepared in small quantities as *metal perchlorates are hazardous and may explode upon heating*!

Synthesis of {Mn-NO}@MCM-41. All manipulations were performed in the dark. A batch of 100 mg of Si-MCM-41 or the Na-exchanged Al-MCM-41 was added to 5 mL of distilled acetonitrile in a 50 mL Schlenk flask containing a magnetic stir bar. The mixture was degassed by three cycles of freeze−pump−thaw, leaving the solution frozen on the last cycle. Next, a batch of 100 or 200 mg of microcrystalline {Mn-NO} was added to the flask under dinitrogen. The solution was then allowed to thaw at room temperature and stirred in the dark for 3 days. The loaded MCM-41 material was collected by filtration using a fritted funnel. The deep green solid was washed with 5 × 2 mL of acetonitrile and 3 × 3 mL of THF. At the end of the repeated washings, the filtrate contained no detectable amount of {Mn-NO} as discerned by electronic absorption spectroscopy. Finally, the light green powder was dried in vacuo.

Samples of Si-MCM-41 loaded by soaking in solutions containing 100 and 200 mg of {Mn-NO} are denoted as $\{Mn\text{-}NO\}_{100}$@Si-MCM-41 and $\{Mn\text{-}NO\}_{200}$@Si-MCM-41, respectively. Similarly, Al-MCM-41 loaded with the solutions containing 100 and 200 mg of {Mn-NO} are denoted as $\{Mn\text{-}NO\}_{100}$@Al-MCM-41 and $\{Mn\text{-}NO\}_{200}$@Al-MCM-41, respectively. {Mn-NO}@MCM-41 is used for referencing all formulations of the loaded material.

Analysis of the Manganese Content of {Mn-NO}@MCM-41. An acid digest procedure modified from the protocol described by Yang and co-workers[41] was used to determine the manganese content of the loaded materials. Batches of 25 mg of the {Mn-NO}@MCM-41 samples were added to the Teflon vessels of autoclave bombs, and to

each was added 1 mL of a 1:3 mixture of concentrated HNO_3 and HCl. The samples were then frozen by dipping the vessels in liquid N_2 before the addition of 0.125 mL of 40% aqueous HF to each vessel. Following addition of HF, the vessels were immediately sealed and allowed to warm to room temperature before placing them in a 150 °C oven for 4 h. Next, the vessels were allowed to cool to room temperature, and 12.5 mg of boric acid was added to each sample solution to complex free F^-. Finally, the samples were diluted to 50 mL using Millipore water containing 1% HNO_3 and transferred to a polypropylene flask for analysis. The total Mn content of each digest solution was measured by flame atomic absorption spectroscopy (FAAS) or inductively coupled plasma-optical emission spectroscopy (ICP-OES). To test the batch-to-batch consistency and the accuracy of the reported loading values for each formulation of the host−guest material, two separate batches of each formulation were synthesized and digested separately, and the Mn content of one digest was measured (in triplicates) by FAAS and the other by ICP-OES. FAAS measurements were performed on a Perkin-Elmer AAnalyst100 with a hollow cathode lamp and filter set to the Mn absorption line of 279.5 nm. The slit width was set to 0.2 nm, and the nebulized digest solution was sent through a nitrous oxide−acetylene flame. ICP-OES measurements were performed on a PerkinElmer Optima 4300DV utilizing the Mn emission line at 259.372 nm and a slit width of 0.2 nm.

Leaching of {Mn-NO} from {Mn-NO}@MCM-41. The extent of the loss of the nitrosyl from the host was checked as follows. Vials containing 5 mg portions of $\{Mn\text{-}NO\}_{200}$@Si-MCM-41 or $\{Mn\text{-}NO\}_{200}$@Al-MCM-41 in 1 mL of 137 mM saline solution were gently agitated for a total time of 24 h. Aliquots of 10 μL were taken from each test solution at various time intervals and brought to 10 mL with Milli-Q water containing 1% HNO_3. Following filtration through a 0.2 μm filter, the Mn content of each sample was determined by ICP-OES analysis. The amount of leached Mn from $\{Mn\text{-}NO\}_{200}$@Si-MCM-41 or $\{Mn\text{-}NO\}_{200}$@Al-MCM-41 for each time point was determined by averaging their values from three independent runs.

The leaching of the photoproduct of {Mn-NO} left in the MCM-41 pores after NO photorelease was also examined. First, samples of {Mn-NO}@MCM-41 were completely photobleached via illumination for 2 h. The completion of this process was confirmed with a NO-specific electrode. Leaching of the Mn-photoproduct (with no bound NO) from such photolyzed samples of $\{Mn\text{-solv}\}_{200}$@Si-MCM-41 and $\{Mn\text{-solv}\}_{200}$@Al-MCM-41 (solv = solvent) in saline solution was then tested by following the procedure described above.

Spectroscopic Measurements. Infrared spectra of the materials (in KBr disks) were recorded on a Perkin-Elmer Spectrum-One FT-IR spectrometer. The absorption spectra were monitored with a Varian Cary 50 spectrophotometer. UV−vis diffuse reflectance spectra (UV−vis DRS) of Si-MCM-41, Al-MCM-41, $\{Mn\text{-}NO\}_{200}$@Si-MCM-41, and $\{Mn\text{-}NO\}_{200}$@Al-MCM-41 were obtained by using a Varian Cary 5000 UV−vis−NIR spectrophotometer (Harrick Praying Mantis diffuse reflectance cell attachment, $BaSO_4$ standard). Samples of each material (∼20 mg) were spread on a bed of $BaSO_4$. The reflectance data were analyzed using the Kubelka−Monk function, and the output of the function was plotted versus the wavelength.

Other Measurements. The structural order of the materials over long-range was assessed by powder X-ray diffraction (PXRD). These measurements were carried out with a Rigaku SmartLab powder diffractometer at a scan rate of 1.5 deg s^{-1} and step size of 0.02 deg. A Micromeritics ASAP 2020 Accelerated Surface Area and Porosimetry Analyzer was used to acquire the nitrogen adsorption and desorption isotherms (at 77 K) of $\{Mn\text{-}NO\}_{200}$@Si-MCM-41 and $\{Mn\text{-}NO\}_{200}$@Al-MCM-41 samples (run in triplicates). Batches of ∼30 mg of the materials were first evacuated at 573 K for 4 h before the measurements. Specific surface areas were calculated using the Brunauer−Emmett−Teller (BET) method[42] while the Barrett−Joyner−Halenda (BJH) method[43] was employed to calculate the pore volume and size distributions. The porosity and volume data of unloaded samples were also analyzed and compared with the data supplied by the manufacturer (Sigma-Aldrich). Cross-sectional analysis of the distribution of the various atoms (Si, O, Al, and Mn) in $\{Mn\text{-}NO\}_{200}$@Si-MCM-41 and $\{Mn\text{-}NO\}_{200}$@Al-MCM-41 was carried out with the aid of scanning electron microscopy coupled with elemental dispersive X-ray spectroscopy (SEM-EDX). The data were collected on a Hitachi HD-2000 dedicated STEM equipped with an Oxford Inca EDS system. The elemental composition of the analyzed area was determined by the Cliff Lorimer thin ratio quantitation method and normalized by total mass of all measured elements to obtain wt % and atomic % for each element. The TEM images were collected at 200 kV accelerating voltage.

NO Release Profile of {Mn-NO}@MCM-41. The NO release profiles of the loaded materials were recorded with a NO-sensitive electrode (inNO-T NO-measuring system, Harvard Apparatus). Samples of ∼10 mg suspension of the {Mn-NO}@MCM-41 in 2 mL of PBS buffer contained in 5 mm diameter vials were used. The release of NO was induced by illumination of the sample with 100 mW/cm^2 light (irradiance intensity measured by a Coherent Field Max II power meter). The samples were exposed to the atmosphere and gently stirred with a microflea stir bar. The tip of the electrode was placed 3 cm above the stir bar, and [NO] was measured at 0.5 s intervals. The amperometric data collected by the electrode were converted into [NO] by calibrating the electrode response during illumination of standard solutions of {Mn-NO} in acetonitrile to the change in concentration of {Mn-NO} by Beer's law analysis at λ = 635 nm. The resulting change in concentration was confirmed to be a result of NO photorelease by the growth of the photoproduct band around 800 nm. The conversion factor obtained (pA to nM of NO) through this method was further confirmed by comparing its value with the results of the standard calibration method of NO formation by an acidified nitrite solution as described by the manufacturer.

The ability of the NO released from {Mn-NO}@MCM-41 to penetrate a 1.1 mm layer of agar (the thickness of the bacterial suspension used in the antibiotic test described below) was assessed using an agar plate containing a 1.1 mm layer of soft agar with dissolved Griess reagent which turns pink in the presence of NO. Samples (10 or 30 mg) of {Mn-NO}@MCM-41 were evenly spread in the center of the agar plates using a template with a circular opening (2.2 cm in diameter) and illuminated for 30 min. The plates were then visualized for the formation of the pink dye on the surface (and beneath) of the agar. The resulting pink circles on the plates demonstrated very little lateral spreading of the released NO from the sites of application.

Growth Conditions for the *A. baumannii* Cultures. Freeze-dried cultures were allowed to thaw and then spread across trypticase soy agar (TSA) plates for growth and isolation single colonies of the bacteria. The TSA plates were grown overnight at 37 °C under aerobic conditions. Following incubation, a single colony was selected, grown in trypticase soy broth (TSB) to an OD_{600} of 0.63 (Varian Cary 50 spectrophotometer) and frozen as working stocks. The conversion factor for calculating CFU mL^{-1} from the OD_{600} for each strain of *A. baumannii* was determined by incubating single-colony isolates in trypticase soy broth (TSB) until OD_{600} = 0.4 and performing dilutions to achieve a density appropriate for cell counting by a hemocytometer. A conversion factor of 2.9×10^8 CFU mL^{-1} per unit of OD_{600} was found for both strains.

Model of Skin and Soft Tissue Infection by *A. baumannii*. Instead of using a typical agar surface covered with bacterial colonies for the antibacterial assays, a model of skin and soft tissue infection was designed through a "bacterial suspension" method.[37] First, the working stock was thawed and an aliquot of 100 μL was added to 1 mL of TSB inside an Eppendorf tube. The tube was then placed on a shaker inside a 37 °C incubator and grown to an A_{600} of 1.40 (late stationary phase). Next, an aliquot of 200 μL of this culture was added to a flask containing 100 mL of "soft brine agar" (0.8% (w/v) agar and 1.0% (w/v) NaCl) kept in the liquid state by storing it in a water bath maintained at 45 °C. The resultant inoculated liquid agar contained 8.1×10^5 cells mL^{-1}. The liquid agar was gently vortexed to obtain a homogeneous suspension of the bacteria, and 6 mL of the inoculated agar was spread over a TSA plate containing 20 mL of 1.5% (w/v) agar. The soft brine agar suspension was allowed to solidify and the plate was then incubated in a 37 °C incubator for 1 h to allow the

Table 1. Wt % of Elemental Mn (and the corresponding wt % of the nitrosyl) Incorporated into Si-MCM-41 and Al-MCM-41 Particles As Determined by ICP-OES and FAAS Measurements

method	$\{Mn\text{-}NO\}_{100}$@Si-MCM-41	$\{Mn\text{-}NO\}_{200}$@Si-MCM-41	$\{Mn\text{-}NO\}_{100}$@Al-MCM-41	$\{Mn\text{-}NO\}_{200}$@Al-MCM-41
ICP-OES (wt %)	1.97(1)	2.04(3)	2.07(1)	2.39(4)
{Mn-NO} (wt %)	19.0(1)	19.7(3)	19.9(1)	23.1(3)
FAAS (wt%)	1.97(2)	2.02(4)	2.15(4)	2.47(4)
{Mn-NO} (wt %)	19.0(2)	19.5(4)	20.1(2)	23.8(4)

microbes to adhere to the agar and form cell-to-cell contacts. Composite agar plates of this kind were used in the bactericidal assays.

Bactericidal Assays. The bactericidal efficacy of $\{Mn\text{-}NO\}_{200}$@Al-MCM-41 was examined on both drug-susceptible and mutidrug-resistant strains of *A. baumannii*. The template with a circular opening (dia = 2.2 cm) was employed to facilitate the application of the powdery material to a well-defined area. The template and the $\{Mn\text{-}NO\}_{200}$@Al-MCM-41 powder used in the test were first sterilized by soaking in 70% ethanol followed by drying at room temperature over 30 min. The template was then placed on top of the inoculated composite agar plate and the desired mass of sterile $\{Mn\text{-}NO\}_{200}$@Al-MCM-41 was evenly spread over the exposed area. Following removal of the template, the whole plate was illuminated with 100 mW/cm^2 of light for the desired duration. After illumination, the MCM-41 powder was gently washed off from the plate with a sterile saline solution and the treated plates were then incubated at 37 °C for 16 h. Control experiments were run following the same procedure but with photolyzed {Mn-solv}@Al-MCM-41 to assess any bacterial clearing due to the host material or any leached Mn-complex. The bactericidal effect of the NO released from the material was assessed by visually comparing the cellular density of the NO-treated plates against the control plates. When complete clearing of the bacterial load was noted, agar samples from the area of application of the {Mn-NO}@MCM-41 material were homogenized and extracted in fresh growth media, plated, and incubated at 37 °C to ensure the lack of any viable bacteria remaining in the kill-zone.

RESULTS AND DISCUSSION

Synthesis and Characterization of {Mn-NO}@MCM-41. In the present work, the manganese nitrosyl has been incorporated into the porous MCM-41 structure by using both silicate- (Si-MCM-41) and aluminosilicate-based (Al-MCM-41) materials. With the neutral Si-MCM-41, the loading of the guest molecule ($[Mn(PaPy_3)(NO)](ClO_4)$) into the porous host as ion pairs is a passive process. The aluminosilicate material Al-MCM-41 with negatively charged aluminum sites was therefore selected to improve the guest loading through an ion-exchange mechanism. Here, the $[Mn(PaPy_3)(NO)]^+$ cations exchange for the Na^+ ions inside the host, and hence the extent of loading is facilitated by a combination of ion exchange and passive diffusion. However, as the load of the nitrosyl guest is increased past the available Al surface sites of the Al-MCM-41 (3 mol % of Al) host, a significant portion of the guest also enters as ion pairs. Loading of both Si-MCM-41 and Al-MCM-41 was performed with a low concentration (100 mg {Mn-NO} per 100 mg MCM-41) and a high concentration (200 mg {Mn-NO} per 100 mg MCM-41) of {Mn-NO} in acetonitrile. The $\{Mn\text{-}NO\}_{200}$@Al-MCM-41 material appears to represent the limit of the loading capacity of the porous Al-MCM-41 material employed in this study because soaking of the host with solutions containing higher (300 mg/5 mL) amount of {Mn-NO} hardly increased the Mn content of the hybrid material.

The actual amount of {Mn-NO} loaded into each material type was determined by an acid digestion followed by analysis of the Mn content of the digest solution by FAAS and ICP-OES. Two batches of each type of material were independently digested and analyzed with the aid of either technique to assess the batch-to-batch consistency and the accuracy of the measurements. The data for the {Mn-NO} contents of {Mn-NO}@ MCM-41 materials are shown in Table 1. As expected, the Al-MCM-41 host was able to load higher amounts of {Mn-NO} when synthesized with both high and low concentrations of soak solution, resulting in materials with compositions of 2.40 wt % Mn (or 1.31 wt % NO) for $\{Mn\text{-}NO\}_{200}$ @Al-MCM-41 and 2.07 wt % Mn (or 1.13 wt % NO) for $\{Mn\text{-}NO\}_{100}$@Al-MCM-41. The composition of the loaded silicate material was determined to be 2.04 wt % Mn (or 1.11 wt % of NO) for $\{Mn\text{-}NO\}_{200}$@Si-MCM-41 and 1.97 wt % (or 1.07 wt % of NO) for $\{Mn\text{-}NO\}_{100}$@Si-MCM-41. The ability of the aluminosilicate material to incorporate a greater amount of {Mn-NO} suggests that the use of a negatively charged material type was indeed effective in promoting guest loading via the more efficient ion-exchange method.

The binding strength of {Mn-NO} to the framework of the Si-MCM-41 and Al-MCM-41 particles was tested by measuring the extent of leaching of {Mn-NO} from the porous structure in a physiologically relevant saline solution (137 mM NaCl). The commonly used PBS buffer was not employed because {Mn-NO} forms an insoluble precipitate in this medium. In such experiments, the loaded materials were soaked in the saline solution and gently agitated for a period of 24 h. Aliquots were taken out at specific intervals, filtered and the amounts of {Mn-NO} in solution were measured by ICP-OES. In a typical measurement after 4 h of soaking, $\{Mn\text{-}NO\}_{200}$@Al-MCM-41 lost 1.91(3)% of the total entrapped guest molecules, while $\{Mn\text{-}NO\}_{200}$@Si-MCM-41 lost 2.34(3)% (Figure S1, Supporting Information). These values are normalized with respect to the total amount of entrapped guest molecules in the materials since the $\{Mn\text{-}NO\}_{200}$@Al-MCM-41 sample, to begin with, had a higher amount of entrapped {Mn-NO} compared to that in $\{Mn\text{-}NO\}_{200}$@Si-MCM-41. These data support the fact that the Al-MCM-41 host does hold the {Mn-NO} guest more tightly within its framework compared to the Si-MCM-41 host. At the end of the 24 h period, the two samples lost 2.92(3)% and 3.44(6)% of the guest nitrosyl, respectively (Figure S1, Supporting Information).

The FTIR spectra of the silicate and aluminosilicate MCM-41 particles exhibit new bands in the region of 1780−1380 cm^{-1} upon loading of {Mn-NO} that demonstrate incorporation of the guest molecule into the host structures. As shown in Figure 1, the incorporated nitrosyl in $\{Mn\text{-}NO\}_{200}$@Si-MCM-41 exhibits ν_{NO} at 1755 cm^{-1} which is shifted slightly to higher energy compared to ν_{NO} of {Mn-NO} (1745 cm^{-1}).[40] Interestingly, if the MCM-41-based materials are not dried properly under high vacuum, the broad water band (δ_{H2O}) at 1630 cm^{-1} often distorts or broadens the ν_{NO} band significantly. The carbonyl group of the ligand frame of {Mn-NO} exhibits its ν_{CO} at 1600 cm^{-1}. This ν_{CO} is red-shifted from 1622 cm^{-1} for the free nitrosyl.[40] In case of $\{Mn\text{-}NO\}_{200}$@Al-MCM-41, the ν_{CO} appears at 1605 cm^{-1} upon incorporation. A

dx.doi.org/10.1021/ja3022736 | J. Am. Chem. Soc. 2012, 134, 11573−11582

similar red shift of ~20 cm^{-1}, previously noted for the adsorption of a polymer containing a carbonyl group onto a silica-based material, has been suggested to arise from interaction of carbonyl groups with the surface hydroxyl groups of the silica platform.[44] It is thus evident that in $\{Mn\text{-}NO\}_{200}$@Si-MCM-41, hydrogen bonding between the polar carbonyl group of the ligand of {Mn-NO} and the hydroxyl groups lining the MCM-41 pores[45] is a significant mode of host−guest interaction. The three bands in the 1350−1500 cm^{-1} region of Figure 1 are assigned ligand pyridine ring vibrations[46] which are all shifted from their respective positions in case of the free nitrosyl. Very similar changes have also been noted in the FTIR spectrum of $\{Mn\text{-}NO\}_{200}$@Al-MCM-41. These data suggest that strong interaction of the polar nitrosyl with the hydroxyl groups on the surface of the pores leads to entrapment of the nitrosyl within the host structure. As discussed below, N_2 adsorption measurements as well as mapping of the various elements in the composite materials also confirm the presence of the nitrosyls *within* the pores of the MCM-41 host.

Diffuse reflectance UV−vis spectroscopy (DRS) was used to confirm {Mn-NO} binding to the Si-MCM-41 and Al-MCM-41. The DR spectra of {Mn-NO}, $\{Mn\text{-}NO\}_{200}$@Si-MCM-41, and $\{Mn\text{-}NO\}_{200}$@Al-MCM-41 are shown in Figure 2 across

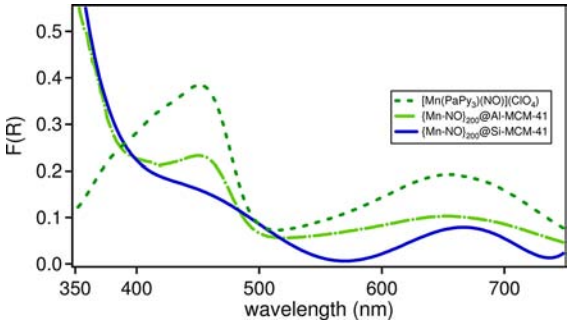

Figure 2. Diffuse reflectance spectra of {Mn-NO} (dashed line), $\{Mn\text{-}NO\}_{200}$@Al-MCM-41 (dash-dot line) and $\{Mn\text{-}NO\}_{200}$@Si-MCM-41 (solid line).

the visible region. The electronic absorption bands of {Mn-NO} appear to broaden and shift slightly upon incorporation into the porous host. Because no drastic change of the nitrosyl DR spectrum is noted compared to those of the loaded materials, it is evident that the coordination structure of the nitrosyl remains intact upon immobilization on the host walls.[47]

The volumetric and porosity changes that occur during loading of the nitrosyl into the MCM-41 materials were determined by comparing the average pore diameter, specific surface area (SSA), and cumulative pore volume of unloaded to loaded Si-MCM-41 and Al-MCM-41 particles. The data for the unloaded particles were obtained from the manufacturer (Sigma- Aldrich) while the data for the loaded particles were determined by N_2 adsorption analysis (Table 2). Both loaded materials demonstrate type-IV N_2 adsorption isotherms with H1-type desorption hysteresis which are characteristic of materials with one-dimensional porous channels (Figure 3). Both samples also show the characteristic inflection in the adsorption isotherm around 0.3 P/P_o from capillary condensation in the MCM-41 mesopores and a multistep desorption isotherm in the region between 0.5 and 0.6 P/P_o indicating a pore blocking effect caused by the loading of {Mn-NO} molecules *within* the pores.[48,49] The BJH cumulative pore

Table 2. Average Pore Diameter, Specific Surface Area (SSA), and Cumulative Volume of Pores of $\{Mn\text{-}NO\}_{200}$@Si-MCM-41and $\{Mn\text{-}NO\}_{200}$@Al-MCM-41 As Determined by N_2 Adsorption Analysis

sample	average pore diameter (Å)	SSA (m^2 g^{-1})	cumulative pore volume (cm^3 g^{-1})
Si-MCM-41	25.02(2)	993.5(7)	0.98(1)
Al-MCM-41	27.50(2)	960.8(6)	1.00(2)
$\{Mn\text{-}NO\}_{200}$@Si-MCM-41	26.51(5)	846.4(4)	0.56(2)
$\{Mn\text{-}NO\}_{200}$@Al-MCM-41	30.48(4)	582.8(2)	0.44(3)

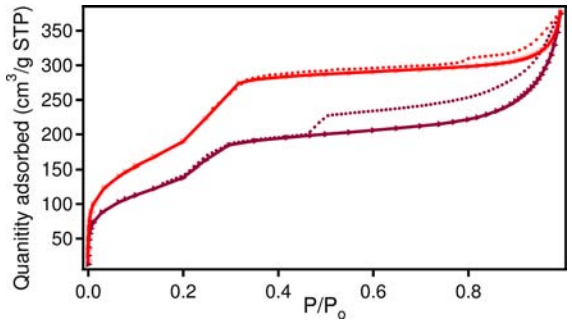

Figure 3. N_2 adsorption (solid line) and desorption isotherms (dotted line) of $\{Mn\text{-}NO\}_{200}$@Si-MCM-41 (red trace) and {Mn-NO}}200@Al-MCM-41 (maroon trace).

volume changes from ~1 cm^3 g^{-1} for the unloaded materials to 0.58 cm^3 g^{-1} and 0.44 cm^3 g^{-1} respectively for Si-MCM-41 And Al-MCM-41 upon loading. These changes indicate a reduction of pore volume by nearly 50% upon incorporation of the nitrosyl. The decrease in pore volume for both materials confirms that {Mn-NO} molecules are being entrapped within the pores of the MCM-41 particles and not simply adsorbed to their exterior surface. The larger change in pore volume upon loading of Al-MCM-41 particles in comparison to that of particles of Si-MCM-41 again demonstrates the higher {Mn-NO} loading efficiency of Al-MCM-41. SSA analysis of Si-MCM-41 and Al-MCM-41 particles using the BET method indicated reductions in the surface area by 153 m^2 g^{-1} and 389 m^2 g^{-1} respectively following nitrosyl loading (Table 2). The relative change in SSA to the change in pore volume was much higher for Al-MCM-41 in comparison to Si-MCM-41. This could arise from stronger binding of {Mn-NO} guests to the negatively charged aluminum sites on the pore surface of Al-MCM-41 particles making the sites inaccessible for adsorption of N_2 molecules during adsorption analysis. In the Si-MCM-41 structure, more loosely bound {Mn-NO} molecules could allow more N_2 molecules to access the binding sites on the wall of the pores.

PXRD analysis was performed on all hybrid materials to determine if the incorporation of {Mn-NO} into the porous framework caused alteration of their structures. The PXRD spectra of unloaded Al-MCM-41 and Si-MCM-41 and loaded $\{Mn\text{-}NO\}_{200}$@Al-MCM-41 and $\{Mn\text{-}NO\}_{200}$@Si-MCM-41 are shown in Figure 4a. The spectra of the unloaded materials display the (100), (110), and (200) reflections that are typical of an ordered mesoporous silicate consisting of a hexagonal array of unidimensional channels.[50] The same peak pattern is observed after loading of the nitrosyls. Despite some loss of crystallinity, the (100) peak is still present, while the higher-angle peaks are slightly above the background. This fact

dx.doi.org/10.1021/ja3022736 | J. Am. Chem. Soc. 2012, 134, 11573−11582

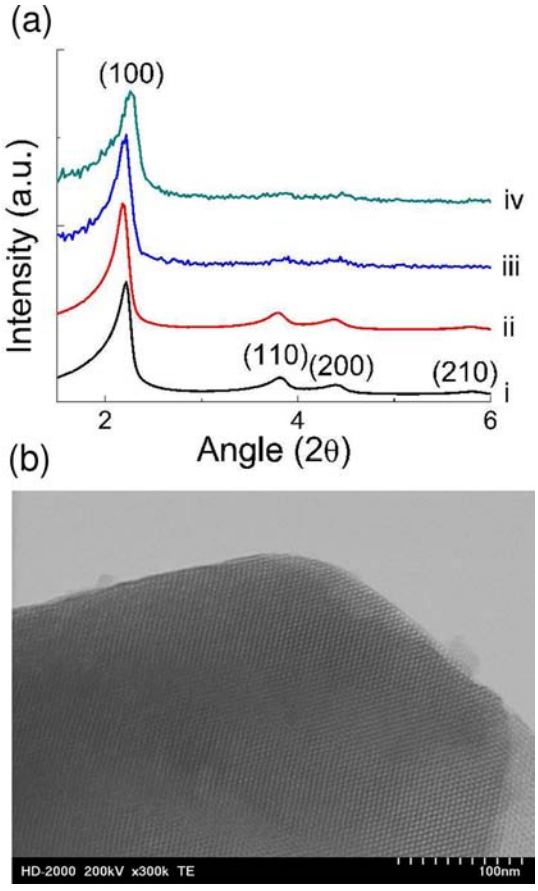

Figure 4. (a) PXRD patterns of: (i) Al-MCM-41 prior to loading; (ii) Si-MCM-41 prior to loading; (iii) $\{Mn\text{-}NO\}_{200}$@Al-MCM-41 after loading; (iv) $\{Mn\text{-}NO\}_{200}$@Si-MCM-41 after loading; (b) TEM micrograph of $\{Mn\text{-}NO\}_{200}$@Al-MCM-41 after loading.

demonstrates that incorporation of {Mn-NO} into the porous framework does not severely alter the MCM-41 structure. Also, the regular array of mesochannels is clearly seen by TEM of the samples after loading (Figure 4b). The loaded materials, however, show a dramatic reduction in peak intensity caused by heavy guest loading in the pores. Such loading decreases the phase contrast between the pore walls and the pore space due to introduction of radiation-scattering matter into the previously void space of the pores.[51]

SEM-EDX elemental mapping was performed on $\{Mn\text{-}NO\}_{200}$@Si-MCM-41 and $\{Mn\text{-}NO\}_{200}$@Al-MCM-41 particles to examine the incorporation of {Mn-NO} into the porous MCM-41 structure and assess the homogeneity of the guest molecule distribution throughout individual particles. Figure 5 shows the cross-sectional SEM-EDX elemental (Si, O, Al, and Mn) maps of a single $\{Mn\text{-}NO\}_{200}$@Al-MCM-41 particle. These maps confirm even distribution of {Mn-NO} throughout the interior of the MCM-41 particle, with the qualitative abundance matching the values expected on the basis of the ICP results. The even spread of Mn across the entire area of the particle indicates that the entire length of the channels traversing the MCM-41 particle are fully accessible to diffusing guest molecules and do not become significantly blocked during the loading process.

NO Release from $\{Mn\text{-}NO\}_{200}$@Si-MCM-41 and $\{Mn\text{-}NO\}_{200}$@Al-MCM-41. Reports thus far on NO release from silicates and other inorganic porous materials have demonstrated NO release only through nontriggered mechanisms, such as the moisture-assisted displacement of NO associated with metal centers in metal-exchanged zeolites,[38,39] or decomposition of NONOates tethered on the surface walls of MCM-41 and related materials.[52] Such mechanisms allow little or no control on the amount or duration of NO release from the material. Because {Mn-NO} releases NO only upon illumination with visible light, we hypothesized that {Mn-NO}@MCM-41 would also demonstrate light-dependent NO release. The behavior of the {Mn-NO}@MCM-41 suspensions in saline solution under illumination with low-power visible light confirmed such expectations. Typical results (of triplicate measurements) are shown in Figure 6. Suspensions of $\{Mn\text{-}NO\}_{200}$@Si-MCM-41 and $\{Mn\text{-}NO\}_{200}$@Al-MCM-41 readily released NO (measured by a NO-specific electrode) when exposed to visible light. The release of NO from these materials was steady under constant illumination (Figure 6, top panel) while periodic exposure resulted in the release of pulses of NO (Figure 6, bottom panel). The latter result confirms complete control of NO release by light triggering. Such behavior is highly desirable in terms of NO delivery because one can deliver a desired dose of NO to a biological target, wait for a certain period of time for observation (via turning off the light), and again repeat the process to study the overall effects of NO more conveniently (vide infra). The NO-releasing capabilities (and stability) of these materials remained intact for at least three months when stored in sealed vials at room temperature in the dark.

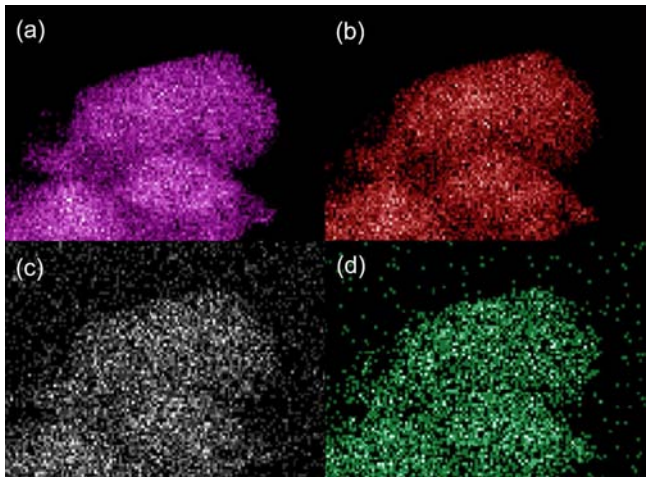

Figure 5. Cross-sectional SEM-EDX maps of Al-MCM-41 after loading: (a) Si; (b) O; (c) Al; (d) Mn.

The NO delivery capacities of $\{Mn\text{-}NO\}_{200}$@Si-MCM-41 and $\{Mn\text{-}NO\}_{200}$@Al-MCM-41 samples were determined with the aid of an inNO-T NO-measuring system. Measurements were performed with suspensions of the materials in saline. As shown in Figure 6 (top panel), a 10 mg sample of $\{Mn\text{-}NO\}_{200}$@Al-MCM-41 afforded a steady level of 70 μM of NO within 5 min of illumination (300 mW visible light), and the level was maintained for 30 min thereafter. At the end of 60 min, the total amount of NO released from the sample (as determined by the Griess reagent) was 4.3(2) μmol, a value very close to the theoretical NO content. With a sample of $\{Mn\text{-}NO\}_{200}$@Si-MCM-41 of similar mass, the level of NO reached a maximum of 50 μM within 5 min. However, the level of photoreleased NO returned to the baseline within 50 min as it entrapped a much lower amount of {Mn-NO} within its

dx.doi.org/10.1021/ja3022736 | J. Am. Chem. Soc. 2012, 134, 11573−11582

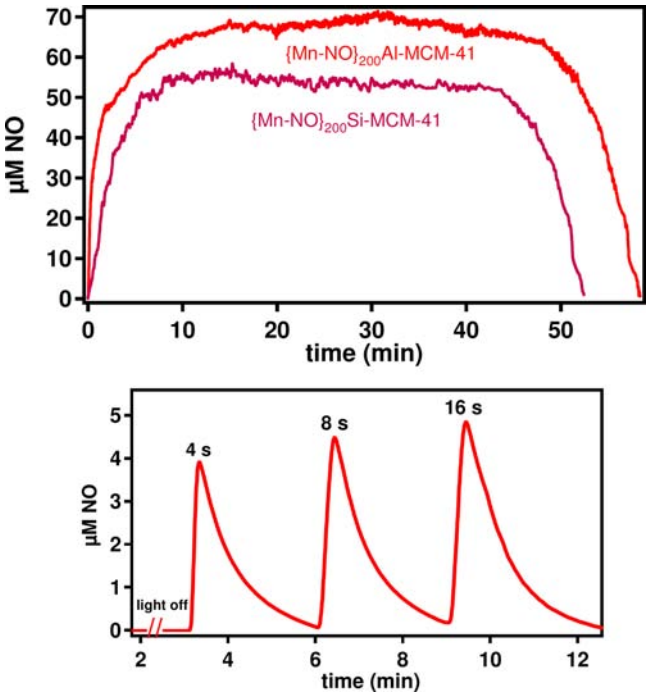

Figure 6. (Top panel): Light-triggered NO release from $\{Mn\text{-}NO\}_{200}$@Si-MCM-41 and $\{Mn\text{-}NO\}_{200}$@Al-MCM-41 suspended in saline solution (constant illumination). (Bottom panel): Bursts of NO release from $\{Mn\text{-}NO\}_{200}$@Al-MCM-41 triggered by light pulses (duration time in s).

porous framework. In a separate experiment, a sample of 5 mg of $\{Mn\text{-}NO\}_{200}$@Al-MCM-41 (suspended in saline) was exposed to light pulses of short duration. As shown in Figure 6 (bottom panel), 4−6 μM bursts of NO were observed with pulse durations of 4−16 s. These results demonstrate that NO release from {Mn-NO}@MCM-41 type of materials can be achieved under the total control of light.

Leaching of the photoproduct of {Mn-NO}, namely $[Mn(PaPy_3)(H_2O)]^{2+}$, was also checked by soaking the NO-spent materials in saline solution and measuring the concentration of manganese (by ICP-OES) in aliquots of the soaking solution. One must note that, following NO photorelease, the entrapped manganese complex turned into a doubly positive species. This change increased the strength of the interaction between the negatively charged aluminum sites of Al-MCM-41 and $[Mn(PaPy_3)(H_2O)]^{2+}$. As a consequence, one observed only trace amounts of leakage of the photoproduct from $\{Mn\text{-}NO\}_{200}$@Al-MCM-41. In the case of $\{Mn\text{-}NO\}_{200}$@Si-MCM-41, such an increase in affinity of the photoproduct toward the host framework was not expected, and indeed the NO-spent material exhibited slightly enhanced leakage of manganese-containing species in saline solution. Strong polar interactions between the photoproduct and the walls of materials, however, exist in both cases, and hence the extent of leakage does not appear to be a significant issue.

Antibiotic Effects of {Mn-NO}@MCM-41 on *A. baumannii*. Following successful incorporation of {Mn-NO} into the porous framework of MCM-41, we have determined the antibiotic potential of the hybrid NO-donor on both a drug-susceptible and a drug-resistant strain of *A. baumannii*. In such attempts, $\{Mn\text{-}NO\}_{200}$@Al-MCM-41 was chosen over the purely siliceous material because of its higher {Mn-NO}-loading capacity and greater NO-releasing ability. The choice also minimized the interference of the potentially cytotoxic Mn complexes on the extent of bacterial clearing due to enhanced retention of entrapped {Mn-NO} and its photoproduct(s). Since {Mn-NO}@MCM-41 powder is intended for the treatment of skin and soft-tissue infections (SSTI) by NO, antibiotic testing was performed using a model designed to mimic the growth environment of skin and soft-tissue and induce bacterial growth and colonization that are representative of SSTI. The SSTI model was constructed by pouring soft-agar (containing $>10^5$ mL^{-1} bacteria) evenly over the surface of a 1.5% TSA plate to create a 1.1 mm thick soft agar layer with homogenously suspended bacteria. This SSTI model served as a useful tool for testing the ability of the NO released from $\{Mn\text{-}NO\}_{200}$@Al-MCM-41 to penetrate the agar matrix and eradicate bacteria at various depths which correspond to the various layers of tissues that are infected by bacteria in SSTIs.

Before any discussion on the bactericidal results, some comments on the SSTI model are warranted. Our SSTI model was designed to address the limitations of the standardized disk diffusion and agar dilution assays for testing the antibiotic efficacy of topical therapies for the treatment of SSTI.[53] The inoculated agar plates used for both of these assays are made by simply spreading a certain amount of liquid culture over the surface of a nutrient rich hard agar plate. Such plates are inadequate for proper antibiotic testing because of several limitations. First, bacteria causing SSTI do not infect the surface of the skin since it comprises mostly dead cells. Instead, the bacteria initially reside in the lower epidermis and the dermis which begins at 0.3 mm.[54] Untreated bacteria in a SSTI continually spread into deeper regions of the cutaneous and subcutaneous tissue through the excretion of exotoxin-like proteases which break down the extracellular matrix of the tissue being invaded.[55] Extremely virulent pathogens such as *A. baumannii* have the ability to move from soft-tissue to the circulatory system through the use of an outer membrane protein (AbOmpA). This protein mediates the interaction of the bacteria with epithelial cells and allows the bacteria to enter the circulatory system where it can then circulate throughout the body and attack key organs, a highly fatal condition called bacterial sepsis.[56] The standardized methods of antibiotic testing contain only surface exposed bacteria and thus are not capable of thoroughly testing the ability of an antibiotic to cause bactericidal effects in the deep tissue regions where the onset of sepsis occurs. Second, these methods are also incapable of invoking the "ditching phenomena" of bacterial penetration into the agar media, because of the abundance of nutrients at the surface.[57] Finally, one of the most important considerations for assessing antibiotics used in the treatment of SSTI is the decreased partial pressure of oxygen which can occur in various subsurface layers of soft tissue, and also upon heavy pathogen colonization of soft-tissue layers. Severely damaged tissues contain damaged microcirculation, increased vessel constriction, and a constant consumption of oxygen from an increase in collagenase activity to repair the damage.[58] The direct administration of antibiotics to surface-exposed bacteria ensures a plentiful source of oxygen, and thus the results of the disk diffusion and agar dilution methods will not include any impact from the effect of oxygen deficiency. The hypoxic conditions that can occur in SSTIs can severely impact the efficacy of certain antibiotics such as tobramycin, amikacin, and aztreonam which demonstrated a 4, 4, and 16-fold increase in their MIC_{50} under hypoxic conditions, respectively.[59] Hypoxic conditions also impact the metabolism of phenotypes of

dx.doi.org/10.1021/ja3022736 | J. Am. Chem. Soc. 2012, 134, 11573−11582

infecting bacteria which often lead to a decrease in bacterial metabolism and, thus, a decrease in cellular uptake of extracellular material (including antibiotics). The partial pressure of oxygen also affects the ability of immune cells to create effective oxidative bursts to combat invading pathogens, a fact that limits the ability of these cells to clear the remaining pathogens after antibiotic adminstration.[58] The SSTI model employed in the present work provides safeguards against all these complications through application of $\{Mn\text{-}NO\}_{200}$@Al-MCM-41 on a soft infected agar layer to test the efficacy of NO (a diffusible small molecule) in reducing the bacterial loads.

A previous study by Mukerji[60] demonstrated the penetration of *A. baumannii* through 1% w/v agar in order to reach a subsurface source of nutrients, suggesting that the subsurface location of the nutrient reservoir (bottom agar layer) in our SSTI model may promote bacterial penetration (ditching) through the soft agar layer. It is known that the subsurface location of the nutrient rich blood vasculature is targeted by a heme-sensing signal transduction system (HbpS) and localize *A. baumannii* around the vasculatures.[61] The 1.1 mm layer of agar in the present SSTI model containing a high concentration of bacteria comprises a nutrient gradient which is at a maximum at the bottom of the 1.1 mm layer. This could promote a high level of metabolic activity leading to a rapid depletion of oxygen in the nutrient-rich areas in a gradient fashion. In addition, the soft agar layer allows mobility of the suspended bacteria so that growth and colonization can occur in a manner similar to that seen in SSTI. In such infections, bacteria can spread in all three dimensions, penetrate deeper into the tissue, and form cell-to-cell contacts, colonies, and biofilms which are all extremely important factors in antibiotic susceptibility.

The results of the antibiotic studies are shown in Figure 7. In the control experiments (plates A and D) with photolyzed $\{Mn\text{-}solv\}_{200}$@Al-MCM-41 powder (with no NO available), the growth of *A. baumannii* was hardly affected. However, the application of 30 mg (plate B) and 50 mg (plate C) of $\{Mn\text{-}NO\}_{200}$@Al-MCM-41 powder on the bacterial lawn caused rapid clearing following 1 h of illumination with visible light. The zone of bacterial clearing caused by photoreleased NO was mostly localized (area in contact with the powder) showing limited lateral diffusion. Facile penetration of NO through the soft agar layer is evident by the complete clearing of bacteria through the entire depth of the agar layer. No viable bacteria were isolated from the cleared areas (as evident by the lack of growth upon transfer of the cleared agar into new growth media) in these experiments. Since the bacterial loads in these experiments mimic the loads one often encounters in clinical cases, deep clearing (reductions of $>10^5$ CFU mL^{-1}) of the loads in the present SSTI model strongly suggests that $\{Mn\text{-}NO\}_{200}$@Al-MCM-41 could be effective in treating *A. baumannii* infections. Encouraging results have also been obtained with the highly drug-resistant strain of *A. baumannii*. With 30 mg of $\{Mn\text{-}NO\}_{200}$@Al-MCM-41 powder, 1 h illumination caused a significant clearing of the bacterial lawn (plate E). When a dose of 50 mg of the hybrid NO-donor was used in conjunction with 1.5 h of illumination time, the clearing was nearly complete (plate F). In plate F, some lateral diffusion of NO is also evident. The increased illumination time for clearing of the more resistant strain indicates that more NO is required to combat such infection. Collectively, these results demonstrate that $\{Mn\text{-}NO\}_{200}$@Al-MCM-41 is an effective bactericidal agent against *A. baumannii* (both drug-susceptible and drug-resistant) grown in a SSTI model. Further *in vivo* studies will, however, be required to confirm its efficacy in treating SSTI infection by these highly problematic Gram-negative bacteria.

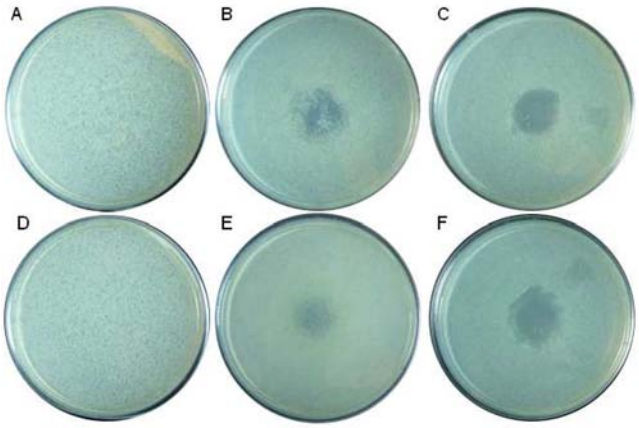

Figure 7. Effects of NO photoreleased from $\{Mn\text{-}NO\}_{200}$@Al-MCM-41 on *A. baumannii* colonies. (A–C): Results with drug-susceptible strain. (D–F): Results with drug-resistant strain. Materials sprayed on the central application zone. (Plate A): Photoproduct showing no reduction of the bacterial load. (Plate B): Clearing of bacterial load with 30 mg of $\{Mn\text{-}NO\}_{200}$@Al-MCM-41. (Plate C): Clearing with 50 mg of $\{Mn\text{-}NO\}_{200}$@Al-MCM-41. (Plate D): Photoproduct effect on the bacteria. (Plate E): Clearing with 30 mg of $\{Mn\text{-}NO\}_{200}$@Al-MCM-41. (Plate F): Clearing with 50 mg of $\{Mn\text{-}NO\}_{200}$@Al-MCM-41.

Studies by Miller and co-workers have shown that doses of 200–300 ppm of NO is nontoxic to key cells involved in tissue repair even when the exposure is continued for 48 h.[62] Exposure to even higher doses of NO for short durations are also tolerated by human cells. In a later study, Miller and co-workers have demonstrated that similar doses of NO are nontoxic to a variety of immune cells, and multiple exposure to NO could be additive to host immune response.[11] In addition, exposure to NO stimulates collagenase expression in fibroblasts.[63] As a consequence, exposure to NO promotes wound healing in addition to its antibiotic effects. We therefore anticipate that application of the {Mn-NO}@MCM-41-type of materials to an infected wound could assist in several ways toward its healing in addition to eradication of the bacterial load.

In summary, loading of a photosensitive manganese nitrosyl into the porous structures of MCM-41 hosts has been achieved in the present work. In case of the neutral Si-MCM-41, the nitrosyl is entrapped within the channels of MCM-41 via interaction with groups on the channel wall. Use of Al-MCM-41 as the host enables one to improve on such loading. In the latter case, the cationic nitrosyl further interacts with the negatively charged Al sites. Leaching of the nitrosyl from these two hosts is minimal in physiological saline. Exposure of these two hybrid materials to visible light results in rapid release of NO from the entrapped nitrosyl while the photoproducts are retained in the host structure. As a consequence, such hybrid NO-donors could be employed to deliver NO under the total control of light with very little toxicity from the biocompatible host that also retains the photoproducts. Such utility has been demonstrated in eradicating *A. baumannii* loads in a SSTI model. Effective clearing of both drug-sensitive and drug-resistant strains of *A. baumannii* has been observed by means of

dx.doi.org/10.1021/ja3022736 | J. Am. Chem. Soc. 2012, 134, 11573–11582

light-triggered NO delivery. With the typical light flux value of 100 mW/cm^2 for a sunny day in mind, we have employed a 100 mW/cm^2 light source in all our measurements. It is expected that application of these nitrosyl-containing porous materials to infected wounds followed by exposure to sunlight will bring about a rapid reduction of the pathogen load. Consequently, powders of this kind could be employed as a first line of treatment for *A. baumannii* infections in battlefield wounds.

■ ASSOCIATED CONTENT

Supporting Information

Plots of {Mn-NO} leaching from the porous hosts with time, and Miller indices and *d*-spacing of peaks observed in the PXRD patterns shown in Figure 4. This material is available free of charge via the Internet at http://pubs.acs.org.

■ AUTHOR INFORMATION

Corresponding Author

pradip@ucsc.edu

Notes

The authors declare no competing financial interest.

■ ACKNOWLEDGMENTS

This research was supported by the NSF Grant DMR-1105296 and a Seed Grant from the California Institute for Quantitative Bioscience (QB3). We thank Prof. Seth Cohen of UC San Diego for providing the facility for gas adsorption measurements. We also thank Dr. Neil Coombs, facility director of the Center of Nanostructure Imaging of University of Toronto for assistance in collecting the elemental maps of the nitrosyl-MCM-41 hybrids. Dr. David Rogow provided help in the diffuse reflectance measurements.

■ REFERENCES

(1) Fang, F. C. *Nitric Oxide and Infection*. Kluwer Academic/Plenum Publishers; New York, 1999.
(2) Halpenny, J. M.; Mascharak, P. K. *Anti-Infect. Agents Med. Chem.* **2010**, *9*, 187−197.
(3) Fang, F. C. *J. Clin. Invest.* **1997**, *99*, 2818−2825.
(4) Fang, F. C. *Nat. Rev. Microbiol.* **2004**, *2*, 820−832.
(5) Gardner, P. R.; Gardner, A. M.; Martin, L. A.; Salzman, A. L. *Proc. Natl. Acad. Sci. U.S.A.* **1998**, *95*, 10378−10383.
(6) Miller, C. C.; Millar, M. K.; Ghaffari, A.; Kunimoto, B. *J. Cutaneous Med. Surg.* **2004**, *8*, 233−238.
(7) Han, G.; Martinez, L. R.; Mihu, M. R.; Friedman, A. J.; Friedman, J. M.; Nosanchuk, J. D. *PLoS ONE* **2009**, *4* (11), e7804.
(8) Mihu, M. R.; Sandkovsky, U.; Han, G.; Friedman, J. M.; Nosanchuk, J.; Martinez, L. R. *Virulence* **2010**, *1*, 62−67.
(9) Ghaffari, A.; Jalili, R.; Ghaffari, M.; Miller, C.; Ghahary, A. *Wound Repair Reg.* **2007**, *15*, 368−377.
(10) Jones, M. L.; Ganopolsky, J. B.; Labbe, A.; Wahl, C.; Prakash, S. *Appl. Microbiol. Biotechnol.* **2010**, *88*, 401−407.
(11) Ghaffari, A.; Miller, C. C.; McMullin, B.; Ghahary, A. *Nitric Oxide* **2006**, *14*, 21−9.
(12) Ormerod, A. D.; White, M. I.; Shah, S. A.; Benjamin, N. *Br. J. Dermatol.* **1999**, *141*, 1051−1053.
(13) Zhang, H.; Annich, G. M.; Miskulin, J.; Osterholzer, K.; Merz, S. I.; Bartlett, R. H.; Meyerhoff, M. E. *Biomaterials* **2002**, *23*, 1485−1494.
(14) Shishido, S. M.; Seabra, A. B.; Loh, W.; de Oliveira, M. G. *Biomaterials* **2003**, *24*, 3543−3553.
(15) Li, Y.; Lee, P. I. *Mol. Pharm.* **2010**, *7*, 254−266.
(16) Riccio, D. A.; Dobmeier, K. P.; Hetrick, E. M.; Privett, B. J.; Paul, H. S.; Schoenfisch, M. H. *Biomaterials* **2009**, *30*, 4494−4502.
(17) Hetrick, E. M.; Schoenfisch, M. H. *Biomaterials* **2007**, *28*, 1948−1956.
(18) Lopez-Jaramillo, P.; Ruano, C.; Rivera, J.; Teran, E.; Salazar-Irigoyen, R.; Esplugues, J. V.; Moncada, S. *Lancet* **1998**, *351*, 1176−1177.
(19) Oh, B. K.; Meyerhoff, M. E. *J. Am. Chem. Soc.* **2003**, *125*, 9552−9553.
(20) Hwang, S.; Meyerhoff, M. E. *Biomaterials* **2008**, *29*, 2443−2452.
(21) Bauer, J. A. *Anticancer Drugs* **1998**, *9*, 239−244.
(22) Halpenny, G. M.; Gandhi, K. R.; Mascharak, P. K. *ACS Med. Chem. Lett.* **2010**, *1*, 180−183.
(23) Chatterjee, D. K.; Fong, L. S.; Zhang, Y. *Adv. Drug Delivery Rev.* **2008**, *60*, 1627−1637.
(24) Taubes, G. *Science* **2008**, *321*, 356−361.
(25) White, A. R. *J. Antimicrob. Chemother.* **2011**, *66*, 1948−1953.
(26) Martínez, J. L.; Rojo, F. *FEMS Microbiol. Rev.* **2011**, *35*, 768−789.
(27) Barraud, N.; Hassett, D. J.; Hwang, S.-H.; Rice, S. A.; Kjelleberg, S.; Webb, J. S. *J. Bacteriol.* **2006**, *188*, 7344−7353.
(28) *Center for Disease Control and Prevention's Report on MRSA Infection*; DOI: 10.3201/eid1604.090107; Centers for Disease Control and Prevention: Atlanta, GA, USA, 2010.
(29) Sengstock, D. M.; Thyagarajan, R.; Apalara, J.; Mira, A.; Chopra, T.; Kaye, K. S. *Clin. Infect. Dis.* **2010**, *50*, 1611−1616.
(30) Van Looveren, M.; Goossens, H. *Clin. Microbiol. Infect.* **2004**, *10*, 684−704.
(31) Peleg, A. Y.; Seifert, H.; Paterson, D. L. *Clin. Microbiol. Rev.* **2008**, *21*, 538−582.
(32) Morgan, D. J.; Liang, S. Y.; Smith, C. L.; Johnson, J. K.; Harris, A. D.; Furuno, J. P.; Thom, K. A.; Snyde, G. M.; Day, H. R.; Perencevich, E. N. *Infect. Control Hosp. Epidemiol.* **2010**, *31*, 716−721.
(33) Fournier, P. E.; Richet, H. *Clin. Infect. Dis.* **2006**, *42*, 692−699.
(34) Centers for Disease Control and Prevention.. *MMWR* **2004**, *53*, 1063−1066.
(35) Murray, C. K.; Roop, S. A.; Hospenthal, D. R.; Dooley, D. P.; Wenner, K.; Hammock, J.; Taufen, N.; Gourdine, E. *Mil. Med.* **2006**, *171*, 826−829.
(36) Scott, P.; Deye, G.; Srinivasan, A.; Murray, C.; Moran, K.; Hulten, E.; Fishbain, J.; Craft, D.; Riddell, S.; Lindler, L.; Mancuso, J.; Milstrey, E.; Bautista, C. T.; Patel, J.; Ewell, A.; Hamilton, T.; Gaddy, C.; Tenney, M.; Christopher, G.; Petersen, K.; Endy, T.; Petruccelli, B. *Clin. Infect. Dis.* **2007**, *44*, 1577−1584.
(37) Heilman, B. J.; Halpenny, G. M.; Mascharak, P. K. *J. Biomed. Mater. Res., Part B* **2011**, *99B*, 328−337.
(38) Wheatley, P. S.; Butler, A. R.; Crane, M. S.; Fox, S.; Xiao, B.; Rossi, A. G.; Megson, I. L.; Morris, R. E. *J. Am. Chem. Soc.* **2006**, *128*, 502−509.
(39) Fox, S.; Wilkinson, T. S.; Wheatley, P. S.; Xiao, B.; Morris, R. E.; Sutherland, A.; Simpson, A. J.; Barlow, P. G.; Butler, A. R.; Megson, I. L.; Rossi, A. G. *Acta Biomater.* **2010**, *6*, 1515−1521.
(40) Ghosh, K.; Eroy-Reveles, A, A.; Avila, B.; Holman, T. R.; Olmstead, M. M.; Mascharak, P. K. *Inorg. Chem.* **2004**, *43*, 2988−2997.
(41) Chao, K. J.; Chen, S. H.; Yang, M. H. *Fresenius' Z. Anal. Chem.* **1988**, *331*, 418−422.
(42) Brunauer, S.; Emmett, P. H.; Teller, E. *J. Am. Chem. Soc.* **1938**, *60*, 309−319.
(43) Barrett, E. P.; Joyner, L. G.; Halenda, P. P. *J. Am. Chem. Soc.* **1951**, *73*, 373−380.
(44) Fontana, B. J.; J. R. Thomas, J. R. *J. Phys. Chem.* **1961**, *65*, 480−487.
(45) Jentys., A.; Kleestorfer., K.; Vinek, H. *Microporous Mesoporous Mater.* **1999**, *27*, 321−328.
(46) Jentys, A.; Pham, N. H.; Vinek, H. *J. Chem. Soc., Faraday Trans.* **1996**, *92*, 3287−3291.
(47) Bottinelli, E.; Miletto, I.; Caputo, G.; Coluccia, S.; Gianotti, E. *J. Fluoresc.* **2011**, *21*, 901−909.
(48) Kresge, C. T.; Leonowicz, M. E.; Roth, W. J.; Vartuli, J. C.; Beck, J. S. *Nature* **1992**, *359*, 710−712.
(49) Hammond, W.; Prouzet, E.; Mahanti, S. D.; Pinnavaia, T. J. *Microporous. Mesoporous Mater.* **1999**, *27*, 19−25.
(50) Breck, D. W. *Zeolite Molecular Sieves*; Wiley: New York, 1974.

(51) Bottinelli, E.; Miletto, I.; Caputo, G.; Coluccia, S.; Gianotti, E. *J. Fluoresc.* **2011**, *21*, 901−909.
(52) Wei, F.; Hou, Q.; Yang, J. Y.; Zhu, J. H. *J. Colloid Interface Sci.* **2011**, *356*, 526−535.
(53) *Clinical and Laboratory Standards Institute Quality Manual*, 3rd ed.; CLSI: Wayne, PA, 2003.
(54) Maton, A, Hopkins, J, McLaughlin, C. W., Johnson, S, Warner, M. Q., LaHart, D, et al. *Human Biology and Health*; Prentice Hall: Englewood Cliffs, 1993.
(55) Moreillon, P.; Que, Y. A. *Lancet* **2004**, *363*, 139−149.
(56) Choi, C. H.; Lee, J. S.; Lee, Y. C.; Park, T. I.; Lee, J. C. *BMC Microbiol.* **2008**, *8*, 216.
(57) Barker, J. *J. Med. Microbiol.* **1975**, *8*, 443−446.
(58) Gottrup, F. *World J. Surg.* **2004**, *28*, 312−315.
(59) King, P.; Citron, D. M.; David, C.; Griffith, D. C.; Lomovskaya, O.; Dudley, M. N. *Diagn. Microbiol. Infect. Dis.* **2010**, *66*, 181−186.
(60) Mukerji. *J. Clin. Pathol.* **1984**, *37*, 103−103.
(61) de Orué Lucana, D. O.; Groves, M. R. *Amino Acids* **2009**, *37*, 479−486.
(62) Ghaffari, A.; Neil, D. H.; Ardakani, A.; Road, J.; Ghahary, A.; Miller, C. C. *Nitric Oxide* **2005**, *12*, 129−140.
(63) Shekhter, A. B.; Serezhenkov, V. A.; Rudenko, T. G.; Pekshev, A. V.; Vanin, A. F. *Nitric Oxide* **2005**, *12*, 210−219.